Relaxation of Ferromagnetic Precession by Excitation of Spin Waves in Polycrystalline Nickel-Cobalt Ferrites

Q. H. F. VREHEN, A. BROESE VAN GROENOU, AND J. G. M. DE LAU

Philips Research Laboratories, N. V. Philips's Gloeilampenfabrieken, Eindhoven, The Netherlands

(Received 7 July 1969)

A detailed test has been made of the spin-wave theory for anisotropy broadening in polycrystalline ferrites. For this purpose, the effective linewidth W and the effective line shift S have been measured as a function of the applied magnetic field, at 9 GHz, for samples of the composition $Ni_{1-x}Co_xMn_{0.05}Fe_{1.95}O_4$, with $x=0$, 0.015, 0.027, and 0.05. For these ferrites, the first-order cubic anisotropy field $2K_1/M_s$ varies from -540 Oe for $x=0$ to $+460$ Oe for $x=0.05$, whereas $4\pi M_s = 3400$ G. The spin-wave theory may thus be expected to be valid. To reduce the influence of porosity on W and S, very dense materials ($p < 0.8\%$) have been used. Well within the limits of the spin-wave manifold, the experimental data are in very good agreement with a theory by Schlömann, except for $x=0$. Near the edges of the manifold, however, the predicted singularities and discontinuities in W and S are not found. It is suggested that this must be attributed to a broadening of the spin-wave frequencies themselves by the variations in the anisotropy field. The amount of this broadening is calculated for a simple model, where the anisotropy field varies sinusoidally. The result for the simple model is then generalized to the case where many Fourier components are present in the anisotropy field. The modifications in the theory lead to an improved agreement with the experiments, especially near the edges of the spin-wave manifold. A further modification of the theory is proposed for the case where the anisotropy field is comparable to or larger than the saturation magnetization. The distribution of anisotropy fields typical for cubic anisotropy must then be introduced into the theory. The theoretical predictions are in fair agreement with recent data of Patton. For pure nickel ferrite, none of the modified theories leads to a good fit with our experiments. This discrepancy remains unexplained. Outside the spin-wave manifold, W has a constant value. At high fields, i.e., below the manifold, W increases linearly with x (16 Oe/% Co). At low fields, the values are higher and not linear in x.

I. INTRODUCTION

LINEWIDTHS for ferromagnetic resonance are usually larger in polycrystalline ferrite samples than in single crystals of the same chemical composition. This line broadening has been ascribed to the presence[1] of voids in the polycrystalline material, and to the random orientation[2] of the crystalline anisotropy axes of the individual crystallites. The present paper is concerned with experimental and theoretical aspects of anisotropy line broadening. We shall assume that the individual grains have cubic anisotropy, of which the order of magnitude is characterized by the quantity $H_a = 2K_1/M_s$, where K_1 is the first-order cubic anisotropy constant and M_s is the saturation magnetization.

In the theories for anisotropy broadening, two limiting cases have been considered. First, when $H_a \gg 4\pi M_s$, one may neglect the dipolar interactions between the magnetizations in different crystallites. If, moreover, the exchange interactions across the grain boundaries are also negligibly small, the various crystallites may be assumed to resonate independently. Such a model is sometimes called an "independent-grain" (IG) model. It has been studied in detail by Schlömann[3] for negative cubic anisotropy ($K_1 < 0$).

Second, when $4\pi M_s \gg H_a$, the anisotropy variations may be neglected at first. The eigenmodes of the homogeneous material are the uniform precession, the magnetostatic modes, and the spin waves. The non-uniformities in the anisotropy field lead to a coupling of the uniform precession to the spin waves, thus to a decrease in the relaxation time of the uniform precession and to a broadening of the ferromagnetic resonance line. This so-called "spin-wave" (SW) model was first proposed by Geschwind and Clogston[4] and investigated for anisotropy broadening by Schlömann.[5] The essential features of the IG model and of the SW model will be discussed in Sec. II.

Experimentally, the SW theory for anisotropy broadening has been tested by the measurement of the linewidth ΔH as a function of frequency,[6] as a function of the shape of the sample[7] or as a function of the orientation of an ellipsoid of revolution in the applied magnetic field.[8] These experiments were in qualitative agreement with the theoretical predictions. A quantitative comparison of theory with experiment was hampered by the fact that the ferrite samples usually had a porosity of a few percent, so that line broadening arising from porosity might dominate the anisotropy broadening.

The technology of ferrite preparation has now improved to such an extent that many materials can be made with porosities well below 1%, so that a better test of the theory should be possible. A better test of the theory has also been made possible by the introduction of the technique in which an "effective linewidth" W is deduced from the microwave susceptibility data over

[1] E. Schlömann, AIEEE Special Publication T-91, 600 (1956).
[2] J. H. van Vleck, Phys. Rev. 78, 266 (1950).
[3] E. Schlömann, J. Phys. Chem. Solids 6, 257 (1958).

[4] S. Geschwind and A. M. Clogston, Phys. Rev. 108, 49 (1957).
[5] E. Schlömann, J. Phys. Chem. Solids 6, 242 (1958).
[6] C. R. Buffler, J. Appl. Phys. Suppl. 30, 172 (1959).
[7] W. Schirmer and K. A. Hempel, Physik Kondensierten Materie 3, 187 (1965).
[8] A. S. Risley, E. G. Johnson, and H. E. Bussey, J. Appl. Phys. 37, 656 (1966); 37, 3646 (1966).

a wide range of magnetic field at a given frequency, rather than the measurement of a linewidth at resonance[6,7] or maximum[8] χ'', only. Kohane and Schlömann[9] deduced the effective linewidth from the imaginary part of the susceptibility for a linearly polarized microwave magnetic field. In that way, W can only be determined sufficiently far-off resonance. More effective is the method in which W is deduced from both the real and imaginary components of the susceptibility. Vrehen[10] introduced this method for a circularly polarized microwave field and Patton[11] used it with a linearly polarized microwave field. Vrehen[10] also measured the "effective line shift" S. The definition and measurement of W and S will be considered in Secs. II and III.

In Sec. IV, we present the experimental results for W and S as measured on a series of ferrites of composition $Ni_{1-x}Co_xMn_{0.05}Fe_{1.95}O_4$ at a frequency of 9.005 GHz for applied magnetic fields between 1600 and 8000 Oe. The cobalt concentrations were $x=0$, 0.015, 0.027, and 0.05. All ferrites had porosities smaller than 0.8%. These compositions have been chosen because the quantity H_a $(=2K_1/M_s)$ varies approximately linearly,[12] from $H_a=-540$ Oe for $x=0$,[13] up to $H_a=+460$ Oe for $x=0.05$, with $H_a\simeq0$ for $x=0.027$.[14] For all values of x, one has $H_a\ll4\pi M_s$. $(4\pi M_s\simeq3400$ G.) The experimental results are therefore compared with Schlömann's SW theory.[5] It will be found that good agreement exists except near the limits of the SW manifold. The remaining discrepancies are most probably due to the perturbations of the SW manifold itself by the anisotropy variations. In Sec. V, a simple model is considered for which W and S can be calculated exactly. The calculation is outlined both in a classical formulation which starts from the equation of motion and in a quantum-mechanical formulation with a Hamiltonian formalism. The result of this calculation for the simplified model is then generalized intuitively for a more realistic situation. Improved agreement with our experiments is obtained. Finally, we propose a further extension of our formulation which gives a reasonable description of S and W in the region $H_a\gtrsim4\pi M_s$. This formulation predicts the parameters S and W for all values of $H_a/4\pi M_s$, i.e., from the SW limit $(H_a\ll4\pi M_s)$ through the intermediate range $(H_a\simeq4\pi M_s)$ up to the IG limit $(H_a\gg4\pi M_s)$, provided that we have $\omega/\gamma\gg H_a$, $4\pi M_s$. This extended theory is compared with experimental data reported by Patton.[11]

II. SOME GENERAL CONSIDERATIONS

In this section, we consider the essential features of the IG model and the SW model, the definition of the experimental parameters W and S, and their physical interpretation. For a uniform isotropic ferromagnet with an internal magnetic field H, derived from an externally applied field H_e, the intrinsic susceptibility χ_+ for a clockwise-rotating microwave magnetic field of angular frequency ω is given by

$$\chi_+=M_s\bigg/\left(H-\frac{\omega}{\gamma}+i\lambda\right). \qquad (1)$$

Here, γ is the gyromagnetic ratio and λ is a relaxation parameter describing the intrinsic damping $(\lambda>0)$. In the limit $\lambda\to0$ we obtain

$$\chi_+=\frac{M_s}{H-\omega/\gamma}-i\pi M_s\delta\left(H-\frac{\omega}{\gamma}\right). \qquad (2)$$

We take into account the presence of magnetic anisotropy by adding to the field H a term $A(\mathbf{r})$, the magnitude of which depends on the position $\mathbf{r}$ because it varies with the grain orientation. The direction of $A(\mathbf{r})$ is supposed to be parallel to H everywhere. In the *independent-grain model*, the susceptibility is then given by

$$\chi_+=\frac{1}{v}\int\frac{M_s}{H+A(\mathbf{r})-\omega/\gamma+i\lambda}d\mathbf{r}, \qquad (3)$$

which in the limit $\lambda\to0$ yields for the imaginary part of χ_+

$$\mathrm{Im}\chi_+\equiv\chi_+''=\pi M_s\left[\frac{1}{v}\int\delta\left(H+A(\mathbf{r})-\frac{\omega}{\gamma}\right)d\mathbf{r}\right], \qquad (4)$$

where v is the volume of the sample. In Eq. (4), the factor between square brackets represents the distribution function of the field $A(\mathbf{r})$. This distribution function completely determines both the real and imaginary part of the susceptibility.

It has been assumed above that the random orientation of the cubic anisotropy axes in the crystallites expresses itself as an additional field $A(\mathbf{r})$ with is parallel to H. In general, this is not correct. If, for a particular crystallite, H does not coincide with a [100], [111], or [110] direction, the equilibrium orientation of the magnetization in that crystallite will not be along H. Moreover, under microwave excitation the magnetization will perform an elliptical precession around its equilibrium position. Schlömann[3] has calculated the susceptibility for negative first-order cubic anisotropy at various values of $\gamma H_a/\omega$. In this paper, we shall, as a rule, assume $H_a\ll\omega/\gamma$, so that Eqs. (3) and (4) may be used.

[9] T. Kohane and E. Schlömann, J. Appl. Phys. **39**, 720 (1968).
[10] Q. H. F. Vrehen, J. Appl. Phys. **40**, 1849 (1969).
[11] C. E. Patton, Phys. Rev. **179**, 352 (1969).
[12] G. Elbinger, Phys. Status Solidi **21**, 303 (1967).
[13] U. Enz and J. Liebertz, Naturwiss. **51**, 54 (1964).
[14] C. M. van der Burgt, Philips Res. Rept. **12**, 97 (1967).

It must be noted that a relaxation time for the uniform precession does not exist in the IG model. After a temporary excitation of the uniform precession by a microwave field, the magnetization in each grain will precess with its own resonance frequency. Phase coherence between the transverse components of the magnetization is lost and thus the "uniform" precession dies out. There is, however, no reason that this should occur exponentially.

In the SW model, one starts from the eigenmodes of a uniform ferromagnet. Only the uniform precession and the SW of small wave number ($k \simeq 10^4$ cm^{-1}) are of interest here. The nonuniformities in the anisotropy field lead to a coupling of the uniform precession to the SW. This results in a frequency shift $\delta\omega$ and a relaxation rate $1/T$ for the uniform precession. In terms of the Fourier components, A_k, of the internal field, defined by

$$H(\mathbf{r}) = H + A(\mathbf{r}) = H + \sum_{\mathbf{k}} A_{\mathbf{k}} e^{i\mathbf{k}\cdot\mathbf{r}}. \qquad (5)$$

T and $\delta\omega$ are given by

$$\frac{1}{T} = \frac{2\pi}{\hbar} \sum_{\mathbf{k}\neq 0} |P_{0\mathbf{k}}|^2 \delta(\hbar\omega - \hbar\omega_{\mathbf{k}}), \qquad (6)$$

and

$$\hbar\delta\omega = \hbar\gamma\langle A(\mathbf{r})\rangle + \sum_{\mathbf{k}\neq 0} |P_{0\mathbf{k}}|^2/(\hbar\omega - \hbar\omega_{\mathbf{k}}), \qquad (7)$$

where $P_{0\mathbf{k}}$ is related to $A_{\mathbf{k}}$ by[5]

$$|P_{0\mathbf{k}}|^2 = \gamma^2 \hbar^2 A_{\mathbf{k}}^2 \cosh^2\mu_{\mathbf{k}}. \qquad (8)$$

Here, $\mu_{\mathbf{k}}$ is defined by

$$\cosh^2\mu_{\mathbf{k}} = \tfrac{1}{2}[1 + (H + Dk^2 + 2\pi M_s \sin^2\theta)/(\omega_{\mathbf{k}}/\gamma)], \qquad (9)$$

where

$$\omega_{\mathbf{k}} = \gamma(H + Dk^2)^{1/2}(H + Dk^2 + 4\pi M_s \sin^2\theta)^{1/2}, \qquad (10)$$

D is the exchange constant, and θ is the angle between $\mathbf{k}$ and H.

We shall assume that the k values of interest are so small that the term Dk^2 may be neglected in (9) and (10). Therefore, $\mu_{\mathbf{k}}$ and $\omega_{\mathbf{k}}$ depend only on θ, and may be written $\mu(\theta)$ and $\omega(\theta)$. The sums in (6) and (7) can be transformed into integrals. The integration over φ and k leads to

$$\frac{1}{T} = \int_0^{\pi/2} \hbar B^2(\theta)\delta(\hbar\omega - \hbar\omega(\theta))\sin\theta\, d\theta, \qquad (11)$$

where

$$B^2(\theta) = \frac{v}{\pi}\cosh^2\mu(\theta)\int_0^\infty k^2\, dk\gamma^2 A_{\mathbf{k}}^2$$

$$= 2\pi\gamma^2\langle A^2\rangle \cosh^2\mu(\theta), \qquad (12)$$

where it has been assumed that $A_{\mathbf{k}}$ is independent of the direction of $\mathbf{k}$.

In Sec. V, the effect of the perturbations on the SW frequencies will be studied. It will be argued that the δ function in (11) has to be replaced by a suitably chosen normalized density-of-state function. As it stands, the δ function in (11) can be integrated easily; with (10) this gives

$$1/T = \omega B^2(\theta_0)/\omega_i\omega_m \cos\theta_0, \qquad (13)$$

where θ_0 satisfies $\omega(\theta_0) = \omega$, $\omega_i = \gamma H$, and $\omega_m = \gamma 4\pi M_s$.

The quantity $\langle A^2\rangle$ can be expressed[5] in terms of the first-order anisotropy constant K_1. If necessary, the second-order constant K_2 can also be used (Sec. V D).

From (13), some essential features of the SW model can be observed: (1) $1/T$ is nonzero only inside the SW manifold which is defined at constant frequency by the range of magnetic field that satisfies

$$\gamma H \leqslant \omega \leqslant \gamma(H^2 + 4\pi M_s H)^{1/2}.$$

(2) $1/T$ has a singularity for $\theta_0 = \tfrac{1}{2}\pi$.

An interesting property of $1/T$ is that the integral of this quantity over frequency is related to the second moment of the absorption line, defined by

$$\langle\omega^2\rangle = \int_0^\infty \chi''(\omega)\omega^2\, d\omega \Big/ \int_0^\infty \chi''(\omega)\, d\omega.$$

From (6), one finds that

$$\int_0^\infty \frac{1}{\gamma T}\, d\omega = \frac{2\pi}{\gamma\hbar^2}\sum_{\mathbf{k}\neq 0}|P_{0\mathbf{k}}|^2 = (\langle\omega^2\rangle - \langle\omega\rangle^2)\frac{2\pi}{\gamma}, \qquad (14)$$

where the second equality has been derived by Schlömann.[5] From (14) and (8) one finds in good approximation[5]

$$\int_0^\infty \frac{1}{\gamma T}\, d\omega \simeq 2\pi\gamma\langle A^2\rangle.$$

Since the experiments are performed at constant frequency, a more useful quantity is the integral of $1/T$ over field. To a good approximation, one has

$$\int_0^\infty \frac{1}{\gamma T}\, dH \simeq 2\pi\langle A^2\rangle. \qquad (15)$$

In this expression, the dipolar effects are a small correction only [for $NiFe_2O_4$ at 9 GHz the result from Eq. (15) is 2% too large]. In Sec. V E a relation similar to (14) for the IG model will be given.

The SW theory leads to two relaxation parameters, namely, the relaxation rate $1/T$ and the frequency shift $\delta\omega$. Experimentally, we measure the real and imaginary parts of the susceptibility χ_+. From these we deduce the effective linewidth W and the effective line shift S according to the following definitions:

$$W \equiv 2M_s \, \mathrm{Im}(1/\chi_+), \tag{16}$$

$$S \equiv H - \omega/\gamma - M_s \, \mathrm{Re}(1/\chi_+). \tag{17}$$

The definitions have been discussed in detail in Ref. 10. In (17), H is the internal magnetic field and χ_+ is the intrinsic susceptibility. For a spherical sample, however, W and S can be deduced from the effective susceptibility and the external magnetic field H_e.[10]

In using (16) and (17) for the determination of W and S from the experimental data, S has always been assumed to be equal to zero for $H_e \geqslant 6$ kOe. This allows a determination of ω/γ from the high-field data, where ω/γ now incorporates any field-independent part of the line shift, e.g., the term $\langle A(\mathbf{r}) \rangle$ in (7).

In terms of the SW model, the quantities W and S have a simple physical meaning as we shall see below. For the IG model, such a simple interpretation does not seem to be possible. However, W and S can always be calculated from the susceptibility as predicted by the IG model with Eqs. (16) and (17), and these predictions can then be compared with the experimental results. This often has an advantage over a direct comparison of the imaginary part of the susceptibility from theory and experiment because χ_+'' has a resonancelike behavior which W does not have.

If a relaxation time does exist for the uniform precession, and this is in particular the case for the SW model, then it can be demonstrated[15] that $W = 1/\gamma T$ and $S = -\delta\omega/\gamma$, where T is the energy relaxation time and $\delta\omega$ is the frequency shift. The field-dependent quantities S and W can thus be compared directly with the predictions of the SW theory. For a discussion of this point, we refer again to our earlier paper.[10]

To give a very direct demonstration of the interpretation of W and S, we present, in Fig. 1, the results for W and S for a single-crystal nickel-ferrite sample. The measurements were made at 9 GHz, room temperature and with $H \| [100]$. W is constant and equal to 10 Oe over a large range of magnetic fields, including the field value for which ferromagnetic resonance occurs (3512 Oe). A large peak is observed at 3434 Oe. This peak arises from the fact that the (310) magnetostatic mode
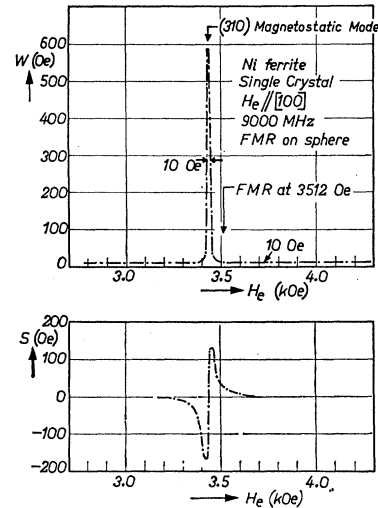

FIG. 1. Effective linewidth W and line shift S as a function of applied magnetic field H_e for a sphere (1.45 mm diam) of a single crystal of $NiFe_2O_4$. H_e was applied parallel to [100]. The sharp variations in W and S are due to the excitation of the (310) magnetostatic mode.

is strongly coupled to the uniform precession as a result of the large diameter (1.45 mm) of the spherical sample used.[16] This peak has a width of just 10 Oe, in agreement with the constant relaxation rate in the sample. Coupling to one mode apparently leads to a narrow resonancelike peak (which would approach a δ function for very small losses) and to a corresponding dispersive resonance in S. According to the SW model, the uniform precession is coupled to a continuum of SW modes, and we may thus expect a broad hump in W extending over the SW manifold.

The usual linewidth ΔH is defined as the difference in field values where χ'' is half its maximum value. Therefore, ΔH is defined over a range of field values, whereas the quantities W and S are known at every H value.[8] An approximate relation between ΔH and W and S is given by

$$\Delta H \simeq W_{\mathrm{res}} + \Delta S, \tag{18}$$

where W_{res} is taken at the field for resonance and ΔS is the difference between the S values found at the field values for half-power absorption.

III. EXPERIMENTAL METHODS

The experimental methods for the determination of W and S have been described in detail in Ref. 10. The real and imaginary parts of the susceptibility χ_+' and χ_+'' are derived from the frequency shift and insertion loss of a cylindrical cavity excited in its TE 112 mode at

[15] C. W. Haas and H. B. Callen, in *Magnetism*, edited by G. T. Rado and H. Suhl (Academic Press Inc., New York, 1963), Vol. I, Chap. 10, pp. 467–470.
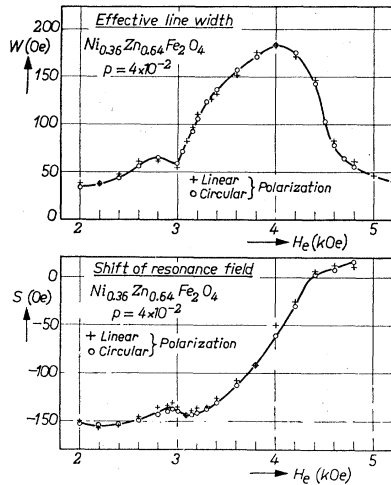
[16] R. Plumier, Physica 28, 423 (1961).

FIG. 2. W and S as a function of magnetic field for a 4% porous polycrystalline $Ni_{0.36}Zn_{0.64}Fe_2O_4$. The results of using linear and circular polarization are compared.
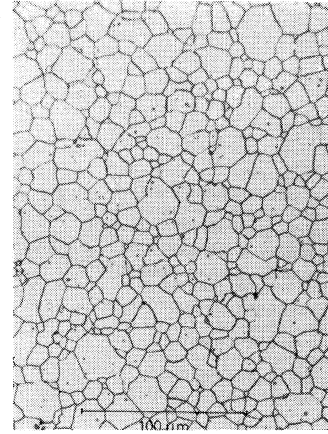

FIG. 3. Photomicrograph of a polished and etched sample of the sintered ferrite of composition $NiMn_{0.05}Fe_{0.95}O_4$. The porosity is 0.36×10^{-2}.

9005 MHz, over a range of external magnetic fields H_e extending from approximately 1600 Oe up to 8000 Oe. All measurements were performed at room temperature. For each material to be investigated, we made measurements on three spherical samples with diameters of roughly 0.6, 1.2, and 2.4 mm. The smallest sample was used for magnetic fields close to resonance, the larger ones for fields farther away from resonance. The uniform precession was driven with a circularly polarized microwave field.

The question is of some interest whether similar results could not also be obtained from measurements with a linearly polarized excitation in a rectangular cavity. From a theoretical point of view X_+ can be interpreted more easily than X_{xx} and thus a direct measurement is to be preferred for samples that have cylindrical symmetry around the z axis. On the other hand, it is easier to measure X_{xx} than X_+, while, moreover, X_+ can be obtained with acceptable accuracy from X_{xx} as follows. Since $X_{\pm} = X_{xx} \pm i X_{yx}$, we have $X_+ = 2X_{xx} - X_-$. In the latter formula X_- represents a rather small correction, which we can take into account approxi-

mately by writing

$$X_-' \simeq M_s \bigg/ \left(H + \frac{\omega}{\gamma} \right) \tag{19}$$

and

$$X_-'' \simeq \left(\frac{H - \omega/\gamma}{H + \omega/\gamma} \right)^2 X_+'' \equiv \alpha X_+''. \tag{20}$$

The approximation of Eq. (20) breaks down for fields close to resonance, but for those fields X_-'' is negligibly small anyway. From Eqs. (19) and (20) we deduce

$$X_+' = 2X_{xx}' - M_s \bigg/ \left(H + \frac{\omega}{\gamma} \right) \tag{21}$$

and

$$X_+'' \simeq 2X_{xx}''/(1+\alpha). \tag{22}$$

With the help of Eqs. (21) and (22), X_+, may be calculated from X_{xx} and then W and S from X_+. To confirm that this procedure works quite well in practice, we measured X_+ directly with our TE 112 cavity, and X_{xx} with a linear TE 102 cavity. W and S as obtained by these two different methods are shown for a porous NiZn ferrite in Fig. 2. Excellent agreement is found.
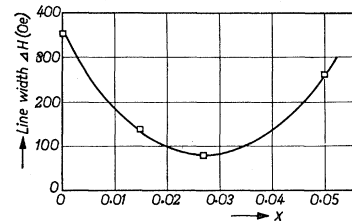
TABLE I. Cobalt content x, porosity p, and anisotropy parameters A_e for $Ni_{0.995-x}^{2+}Co_x^{2+}Mn_{0.005}^{2+}Fe_{1.955}^{3+}Mn_{0.045}^{3+}O_4$.

x	p	$2K_1/M_s$ (Oe)	A_e(expt) (Oe)	A_e(theor) (Oe)
0	0.36×10^{-2}	-540	340	320
0.015	0.20×10^{-2}	-250	150	172
0.027	0.7×10^{-2}	0	68	90
0.050	0.8×10^{-2}	$+460$	260	245

FIG. 4. Ferromagnetic resonance linewidth, measured at 9 GHz, versus Co content for $Ni_{0.995-x}^{2+}Co_x^{2+}Mn_{0.005}^{2+}Fe_{1.955}^{3+}Mn_{0.045}^{3+}O_4$.
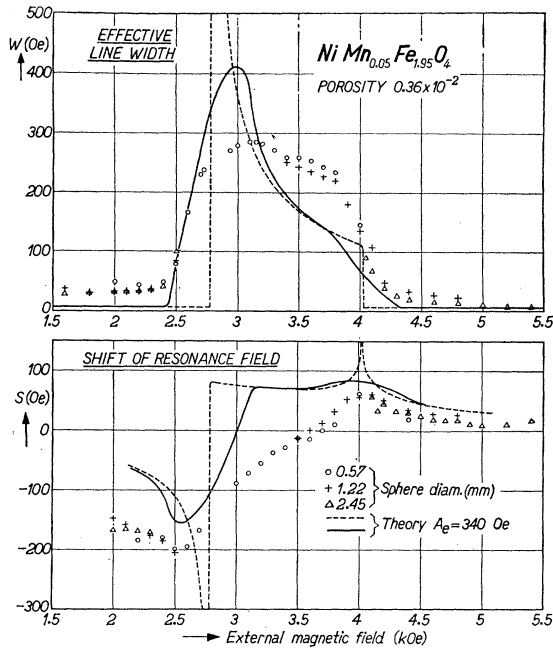
FIG. 5. W and S versus external magnetic field for $NiMn_{0.05}$ $Fe_{1.95}O_4$. The dashed line has been drawn according to (6) and (7). A constant intrinsic damping has been added, so as to bring theory in agreement with experiment at high magnetic fields. The drawn line follows from the theory in Sec. V, where the intrinsic damping has been incorporated into the equations of motion.

In the Introduction, it was emphasized that the test of the anisotropy broadening theory depends critically on the availability of very dense materials and therefore a few words will now be said about the preparation of the ferrites.
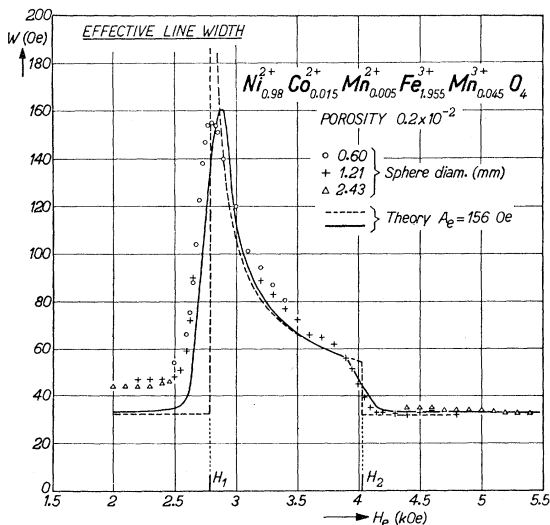

FIG. 6. W versus H_e for $Ni_{0.98}^{2+}Co_{0.015}^{2+}Mn_{0.005}^{2+}Fe_{1.955}^{3+}$ $Mn_{0.045}^{3+}O_4$; lines as in Fig. 5.
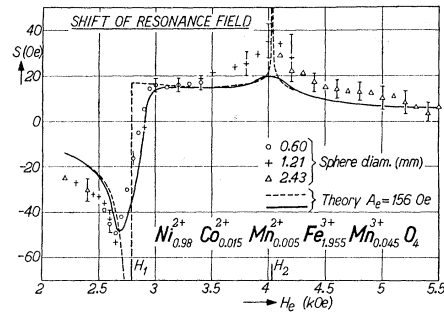
FIG. 7. S versus H_e for $Ni_{0.98}^{2+}Co_{0.015}^{2+}Mn_{0.005}^{2+}Fe_{1.955}^{3+}$ $Mn_{0.045}^{3+}O_4$; lines as in Fig. 5.

Dense and homogeneous materials have been made by the following techniques. Sulphate spray drying and roasting[17,18] were used for the preparation of the powders, which were then compacted by hydrostatic pressing at 1000 kg/cm². The final sintering was carried out at 1250°C for 22 h in a pure oxygen atmosphere. The special method of powder preparation combines the advantages of a high degree of chemical purity and homogeneity with excellent sintering properties.

The density of the final product was measured on 10 g of material by weighing both in air and in water. After correction for the influence of the temperature on the density of the water, the density can be determined within 0.1%. In all cases, densities larger than 99% of the x-ray density were obtained (Table I).

The microstructure was determined on polished and etched samples. Figure 3 shows a regular structure with an average grain size of about 10 μ.

The electrical resistivity was measured by the four-point compensation method. The values found lie in the range between 10^8 and 10^9 Ω cm.
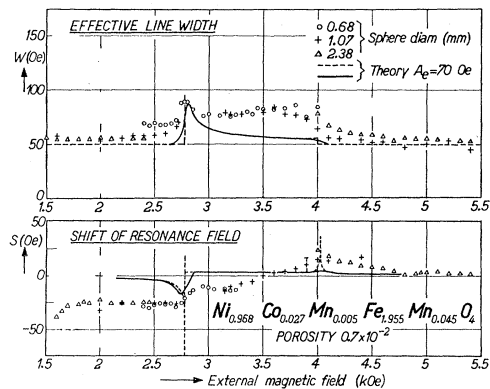

FIG. 8. W and S versus H_e for $Ni_{0.968}^{2+}Co_{0.027}^{2+}Mn_{0.005}^{2+}$ $Fe_{1.955}^{3+}Mn_{0.045}^{3+}O_4$. Lines as in Fig. 5.

[17] J. G. M. de Lau, Klei en Keramiek **19**, 86 (1969) (in Dutch).
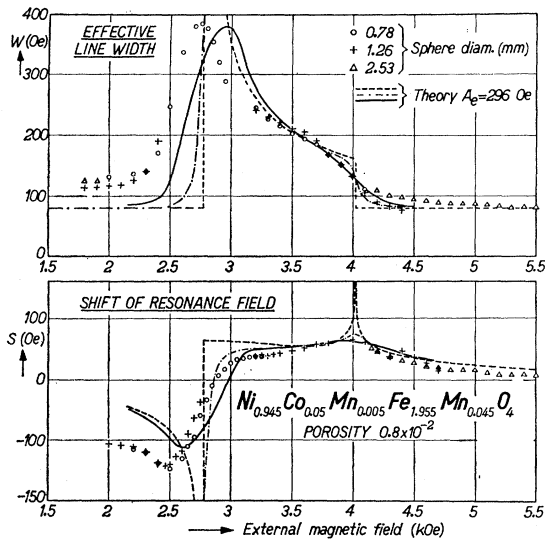[18] J. G. M. de Lau, Seventy-First Meeting of the American Ceramics Society, 1969 (unpublished).

FIG. 9. W and S versus H_e for $Ni_{0.945}{}^{2+}Co_{0.05}{}^{2+}Mn_{0.005}{}^{2+}Fe_{1.955}{}^{3+}Mn_{0.045}{}^{3+}O_4$. The dashed line as in Fig. 5; the dot-dashed line has been drawn according to first-order theory, taking into account an intrinsic damping of 80 Oe.

IV. EXPERIMENTAL RESULTS

For a series of NiCo ferrites, data were taken of the linewidth at resonance. The results, shown in Fig. 4, are similar to those obtained by Sirvetz and Saunders.[19] The minimum is due to the variation of K_1 through zero. Quantitatively these results will be discussed in Sec. V.

In Figs. 5–9, data on W and S are given as obtained from the experimental results on the susceptibility, using Eqs. (16) and (17). A preliminary account has been given before.[20]

According to the considerations given in Sec. II, large W and S values are expected when the uniform precession is degenerate with long-wavelength SW. For a frequency of 9.005 GHz and $\gamma/2\pi = 3.10$ the limits of the SW manifold are found at $H = 2.8$ kOe ($\theta_k = 90°$) and at $H = 4.0$ kOe ($\theta_k = 0°$).

Qualitatively, the experimental results agree with theory. At low fields (between 1.6 and 2.5 kOe), small values of W and S are found. S is negative. Here, the operating frequency is above the frequency for $\theta_k = 90°$ spin waves.

At fields between 2.5 and 4.2 kOe, W and $|S|$ are much larger, while S becomes positive. In this range, the uniform precession is degenerate with $k \simeq 0$ spin waves. The third range is found for fields between about 4.2 and 8 kOe, which is the highest-field value where meaningful values of the damping could be measured. In this high-field range, the value of W is found to be small, but constant, whereas S decreases to zero.

Since a constant level of W is found at low and high fields, we shall first consider these two ranges together. A quantitative description of the anisotropy effects within the SW manifold will be given in the last part of this section.

The W values at $H = 2$ kOe and $H = 6$ kOe were taken as representative of the low- and high-field values, respectively. Figure 10 shows the variation of these values with Co concentration x.

For the 6-kOe data, a linear relation between W and x is found, with a slope of 16 Oe/% Co. These data have been taken below the SW manifold, where anisotropy broadening is absent. Therefore, it is possible to compare these data with the value of the linewidth measured on single crystals, where anisotropy broadening is also absent. Linewidth data on Co-substituted $NiFe_2O_4$ have been published by Smith and Jones,[21] who found $\Delta H = 18$ Oe/% Co, and by Miyamoto, Tanaka, and Iida,[22] who reported $\Delta H = 8$ Oe/% Co. The reason for this discrepancy is not clear. Our results clearly favor Smith and Jones's data.

These data can also be compared with the SW linewidth ΔH_k obtained by parallel pumping. At 9 GHz, Beljers found with our samples the values of ΔH_k given in Fig. 10. Again, a linear relation is found, the slope being 10 Oe/% Co. Taking into account that the SW frequency in this experiment is half that of the pumping frequency, one may conclude that the influence of Co on damping seems to be a nearly linear function of frequency.

The effects of Co on the relaxation of the uniform precession have been discussed in terms of two-magnon processes.[15] From our experiments one may conclude that such processes do not play an important part. In this connection it should be noted that Teale[23] arrived at the same conclusion from his experimental results on single crystals of Co-substituted $MnFe_2O_4$.

At field values below 2.5 kOe the W curves are systematically higher than the curves at higher fields. The difference between the W values at 2 kOe and those at 6 kOe is seen in Fig. 10 to be a minimum at $x = 0.027$, where $|K_1|$ is smallest. This suggests that anisotropy broadening is still present when the exciting frequency is above the $\theta = 90°$ SW frequency. Such a broadening might be due to scattering to $k \neq 0$ SW.

In the following, the high-field values of W will be used as the intrinsic damping parameter of both the uniform precession and the spin waves. In order to compare the experimental results with anisotropy broadening theory, this intrinsic damping has to be taken into account. In most cases this can be done by adding the high-field W value to the theoretical W values.

[19] M. H. Sirvetz and J. H. Saunders, Phys. Rev. **102**, 366 (1956).
[20] Q. H. F. Vrehen, A. Broese van Groenou, and J. G. M. de Lau, Solid State Commun. **7**, 117 (1969).

[21] A. B. Smith and R. V. Jones, J. Appl. Phys. **37**, 1001 (1966).
[22] S. Miyamoto, N. Tanaka, and S. Iida, J. Phys. Soc. Japan **20**, 753 (1965).
[23] R. W. Teale, J. Appl. Phys. **33**, 1295 (1962).

Our experimental results within the manifold will now be compared with the theoretical expressions (12) and (13) which are shown as dashed lines in Figs. 5–9.

Good quantitative agreement is found in Figs. 6, 7, and 9. In Fig. 5, the shape of the experimental W and S curves is quite different from that of the dashed lines.

Rather low S and W values are found in Fig. 8, which is in agreement with the low anisotropy constant K_1 for this compound.[14] The small amount of porosity present ($p = 0.7 \times 10^{-2}$) may now contribute substantially to the relaxation. We attribute the broad maximum in the W curve at $H = 3.8$ kOe to porosity broadening. The W value, 30 Oe above the high-field level of 50 Oe, is in reasonable agreement with the value deduced from measurements on porous NiZn ferrites.[10] In Fig. 8, the drawn curve is the result of anisotropy broadening theory, using the intrinsic damping of 50 Oe and $H_a = 110$ Oe. The curve gives a reasonable description of two pecularities in the W and S curves at 2.8 kOe—a step in S of 20 Oe and a narrow peak in W of 36 above the high-field level. In Sec. V D, the second-order anisotropy constant K_2 will be shown to be responsible for this large value of H_a.

The dashed lines in Figs. 5–7, and 9 do not agree with the experimental results in a range of fields around the limits of the SW manifold. In particular, the predicted infinite peak at $H = 2.8$ kOe is not found, although pronounced maxima are present in both S and W curves.

As for the peak, Schlömann[5] has already shown that the presence of some intrinsic damping removes the singularities. Taking for the intrinsic damping the value of W at high fields, we find for $x = 0.05$ that the theoretical curve is changed, as shown by the dot-dashed line in Fig. 9. At $H = 2.8$ and 4.0 kOe the curves are somewhat rounded off, but the peak remains too high in comparison with experiment. Since the intrinsic damping for the other compositions is even smaller, it cannot remove the disagreement.

In Figs. 5, 6, and 9, W is seen to decrease to its low "intrinsic" values outside the SW manifold over a range of fields, which equals about 500 Oe for Figs. 5 and 9 and about 250 Oe for Fig. 6. These values are of the order of magnitude of the anisotropy field.

In Sec. V, a simple extension of the theory will be presented in order to improve on these details of the S and W curves.

V. ANISOTROPY BROADENING THEORY

A. Simple-Model Equation-of-Motion Calculation

In Sec. IV the experimental data were seen to fit Schlömann's anisotropy theory closely if the frequency of the uniform precession is well inside the limits of the SW manifold. The experimental results showed also that the edges of the manifold are not as sharp as the
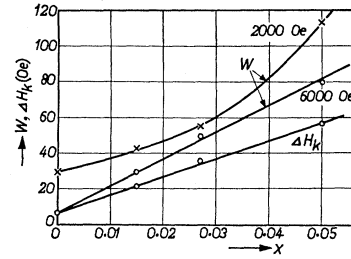
FIG. 10. W at 6 kOe, W at 2 kOe and SW linewidth ΔH_k from parallel pumping instability versus Co content x.

first-order theory assumes, which is not surprising in view of the nonuniform anisotropy field.

It is of interest to calculate the influence of a nonuniform field in detail. For the simple case of one Fourier term in the internal field we will show that the SW frequencies are broadened, by the interactions between the spin waves. This broadening affects the relaxation of the uniform precession to the spin waves.

In order to calculate this effect, we consider an ellipsoidal sample in a static magnetic field. Around the field direction there is cylindrical symmetry, the transverse demagnetization coefficient being N. Suppose that the anisotropy adds to the z component of the internal field, H, a simple cosine variation, so that

$$H(\mathbf{r}) = H + A_q \cos(\mathbf{q} \cdot \mathbf{r}). \qquad (23)$$

The angle between $\mathbf{q}$ and the direction of H will be called θ_q.

There are several ways of obtaining the influence of the cosine term in (23) on the uniform precession. First, we shall use the method of the equation of motion, leading to a solution which includes intrinsic damping. In Sec. V B, a transition probability calculation will be given, an approach that can more easily be extended to the case where many Fourier components are present (Sec. V C), or where the cubic character of the anisotropy energy has to be introduced explicitly (Sec. V E).

The equation of motion reads

$$\frac{1}{\gamma} \frac{\partial \mathbf{M}}{\partial t} = \mathbf{M} \times \mathbf{H}_{eff} - \frac{\alpha}{\gamma |\mathbf{M}|} \mathbf{M} \times \frac{\partial \mathbf{M}}{\partial t}, \qquad (24)$$

where $\mathbf{M}$ is the sum of a small component $\mathbf{m}(\mathbf{r},t)$, perpendicular to the z axis, and a component along the z axis, which is assumed constant and equal to the saturation magnetization M_s in the linear approximation. $\mathbf{H}_{eff}$ includes the static field $\mathbf{H}(\mathbf{r})$ given by (23), the applied uniform microwavefield $\mathbf{h}^{(e)}$, perpendicular to H, and the demagnetizing field $\mathbf{h}^{(d)}(\mathbf{r},t)$. The contribution of exchange to H_{eff} will be neglected. The quantity α is the damping parameter. In the absence of propagation effects $\mathbf{h}^{(d)}$ satisfies Maxwell's equation

$$\text{div}\,\mathbf{b} = \text{div}[\mathbf{h}^{(d)} + 4\pi \mathbf{m}(r)] = 0, \quad \text{rot}\,\mathbf{h}^{(d)} = 0 \qquad (25)$$
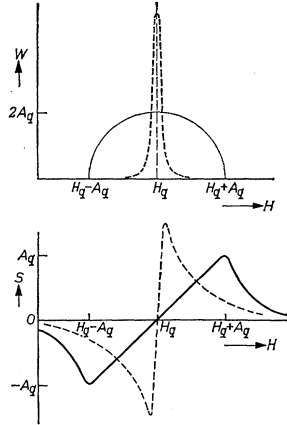
FIG. 11. W/A_q and S/A_q versus magnetic field H as calculated for a sinusoidally varying anisotropy field. The dashed line is for first-order theory, the drawn lines for the exact solution. H_q is the field value for which $\omega=\omega_q$ in Eq. (28).

and the appropriate boundary conditions on the surface of the sample.

The stationary solutions of (24) and (25) at frequency ω, $\mathbf{m}(\mathbf{r},t)=\mathbf{m}(\mathbf{r})e^{i\omega t}$, are known to be given, for $A_q=0$, by the uniform precession, the magnetostatic modes and the short-wavelength SW. Since the wave vector $\mathbf{q}$ of the perturbation is much larger than the inverse of the sample dimensions, the coupling to the magnetostatic modes is weak and will be neglected.

In this approximation, div$\mathbf{m}$ consists of a contribution from the bulk due to the spin waves and one from the surface due to the uniform precession.

In terms of the Fourier components of $\mathbf{m}$, given by

$$\mathbf{m}(\mathbf{r})=\sum_{\mathbf{k}}\mathfrak{m}(\mathbf{k})e^{i\mathbf{k}\cdot\mathbf{r}},\qquad(26)$$

the expression for $\mathbf{h}^{(d)}$ can easily be written

$$\mathbf{h}^{(d)}=-4\pi\sum_{\mathbf{k}\neq0}\{\mathbf{k}[\mathfrak{m}(\mathbf{k})\cdot\mathbf{k}]/|\mathbf{k}|^2\}e^{i\mathbf{k}\cdot\mathbf{r}}-4\pi N\mathfrak{m}(0).\quad(27)$$

In the Appendix, it will be shown that the solution of (24) and (27) contains Fourier components with $\mathbf{k}=n\mathbf{q}$ only. The susceptibility $X_+(0)$ can then be calculated, which yields the quantities S and W.

In a first-order approximation, one restricts the series to the terms with $n=0, \pm1$. Figure 11 shows schematically the results for S and W of this first-order theory by the dashed lines. These curves are typical for the coupling to one single mode (compare Fig. 1) at a frequency:

$$\omega_q=\omega(\theta_q)=\gamma H^{1/2}(H+4\pi M_s\sin^2\theta_q)^{1/2}.\qquad(28)$$

Equations (27) and (28) can also be solved exactly. The details of the calculation are given in the Appendix. The results for negligible intrinsic damping are shown in Fig. 11 by the drawn lines. Instead of a sharp loss peak at one single-field value, a range of fields is found

where W is nonzero. The width of this region equals the total spread in internal field, $2A_q$. The same value is found for the maximum of W, which is apparently not reduced by dipolar narrowing. Such narrowing is found only when the anisotropy variations occur in many directions. This will be shown in Sec. V C.

B. Simple-Model Transition-Probability Calculation

Here, we shall present a quantum-mechanical treatment of the problem formulated in Sec. V A. We describe the system by a Hamiltonian $\mathfrak{IC}=\mathfrak{IC}_0+V$, where $\mathfrak{IC}_0$ is the unperturbed Hamiltonian for a uniform internal field H, and V presents the perturbation by the anisotropy field $A(\mathbf{r})=A_q\cos(\mathbf{q}\cdot\mathbf{r})$. For reasons already outlined in Sec. V A, we may restrict ourselves to the set of SW with wave vectors $n\mathbf{q}$, where n is any integer. We also assume that the contribution from the exchange interaction to the SW energy may be neglected. All spin waves of the set with $n\neq0$ then have the same energy $\hbar\omega_q$. The energy of the uniform procession $\hbar\omega_0$, however, may differ from $\hbar\omega_q$, since surface demagnetization affects ω_0 and volume demagnetization influences ω_q. Thus,

$$\mathfrak{IC}_0=\hbar\omega_0(b_0{}^\dagger b_0+\tfrac{1}{2})+\sum_{n\neq0}\hbar\omega_q(b_n{}^\dagger b_n+\tfrac{1}{2}),\qquad(29)$$

where $b_n{}^\dagger$ and b_n are the creation and annihilation operators for spin waves with wave vector $n\mathbf{q}$. In the perturbation V we distinguish between three different parts V_1, V_2, and V_3, as follows:

$$V_1=-(\tfrac{1}{2}\gamma\hbar A_q)\cosh\mu_q$$
$$\times(b_0{}^\dagger b_1+b_0b_1{}^\dagger+b_0{}^\dagger b_{-1}+b_0b_{-1}{}^\dagger),$$

$$V_2=-(\tfrac{1}{2}\gamma\hbar A_q)\sum_n{}'(\cosh^2\mu_q+\sinh^2\mu_q)$$
$$\times(b_n{}^\dagger b_{n+1}+b_{n+1}{}^\dagger b_n),\qquad(30)$$

$$V_3=(\tfrac{1}{2}\gamma\hbar A_q)\sum_n{}'2\cosh\mu_q\sinh\mu_q[\exp(2i\phi_q)b_n{}^\dagger b_{-n-1}{}^\dagger$$
$$+\exp(-2i\phi_q)b_{-n}b_{n+1}].$$

The primed summation is over all $n\neq0$, ±1. The quantity μ_q is defined in Eq. (9). The angles ϕ_q and θ_q are the polar angles of the vector $\mathbf{q}$. Expression (30) becomes particularly simple for $H\gg4\pi M_s$, because in that limit $\cosh\mu_q\sim1$ and $\sinh\mu_q\sim0$.

In (30), V_1 describes the interaction of the uniform precession with the SW system, whereas V_2 and V_3 present interactions between spin waves. It should be noted that within our approximations the various terms in V_2 do conserve energy, whereas those in V_3 do not. V_3, moreover, contains the factor $\sinh\mu_q$ which becomes small for ω larger than ω_m. Therefore, we shall disregard V_3 in the remainder of the discussion.

The Hamiltonian $\mathfrak{IC}_0+V_1+V_2$ can easily be diagonalized exactly if $\omega_0=\omega_q$. One finds new states

whose energy is spread, approximately, from $\omega_q - \gamma A_q$ up to $\omega_q + \gamma A_q$. From the new states one may derive the tensor susceptibility χ_+ and from this the effective linewidth W and the effective line shift S. The results are very similar to those obtained in Sec. V A.

It seems of more interest to follow a slightly different approach here. We first diagonalize the Hamiltonian $\mathcal{3C}_0 + V_2$. This procedure leaves the uniform precession unaffected, but it yields new spin-wave states whose energies are spread around ω_q. Next, the consequences for the uniform precession are investigated by taking V_1 into account as a perturbation. Transition probability theory yields the energy relaxation time T, and perturbation theory, the frequency shift $\delta\omega$. This approach is more closely related to the usual treatment of the SW model. The diagonalization of $\mathcal{3C}_0 + V_2$ can be realized by the introduction of new creation and annihilation operators $c_{\varphi,\pm}^\dagger$ and $c_{\varphi,\pm}$, which are functions of the continuous variable φ and of a discrete variable taking on the values $+$ and $-$. The relations between the $c_{\varphi,\pm}^\dagger$ and the $b_{\pm n}^\dagger$ are

$$c_{\varphi,\pm}^\dagger = (2/\pi)^{1/2} \sum_{n=1}^{\infty} b_{\pm n}^\dagger \sin n\varphi, \quad 0 \leq \varphi \leq \pi \quad (31)$$

and

$$b_{\pm n}^\dagger = (2/\pi)^{1/2} \int_0^\pi c_{\varphi,\pm}^\dagger \sin n\varphi \, d\varphi, \quad n=1,2,\ldots \quad (32)$$

with similar expressions for the annihilation operators. We then have

$$\mathcal{3C}_0' + V_1' = \hbar\omega_0(b_0^\dagger b_0 + \tfrac{1}{2}) + \sum_{+,-} \int_0^\pi E_\varphi(c_{\varphi,\pm}^\dagger c_{\varphi,\pm} + \tfrac{1}{2}) d\varphi$$

$$- (\tfrac{1}{2}\gamma\hbar A_q) \sum_{+,-} (2/\pi)^{1/2} \int_0^\pi (b_0 c_{\varphi,\pm}^\dagger + b_0^\dagger c_{\varphi,\pm})$$

$$\times \cosh\mu_q \sin\varphi \, d\varphi, \quad (33)$$

where

$$E_\varphi = \hbar\omega_q + \gamma\hbar A_q(\cosh^2\mu_q + \sinh^2\mu_q) \cos\varphi. \quad (34)$$

The last part of the Hamiltonian (33) is treated as the perturbation which couples the uniform precession to the states $(\varphi,\pm)$. The transition probability can now be obtained in the standard way (see, e.g., Ref. 24). The result is

$$\frac{1}{T} = 2\frac{2\pi}{\hbar}\frac{2}{\pi}\int_0^\pi \sin^2\varphi \, \delta(\hbar\omega_0 - \hbar\omega_\varphi)$$

$$\times (\tfrac{1}{2}\gamma\hbar A_q)^2 \cosh^2\mu_q d\varphi. \quad (35)$$

[24] M. Sparks, *Ferromagnetic Relaxation Theory* (McGraw-Hill Book Co., New York, 1964).

The first factor of 2 arises from the scattering to states φ_+ and φ_- which are degenerate. Performing the integration yields

$$1/T = 2(2\pi/\hbar)(\tfrac{1}{2}\gamma\hbar A_q)^2 \cosh^2\mu_q \{(2/\pi)[(\gamma\hbar A_q)^2\eta_q^2 - (\hbar\omega_0 - \hbar\omega_q)^2]^{1/2}/(\gamma\hbar A_q\eta_q)^2\}, \quad (36)$$

where ω_0 must be restricted to values at which the expression under the square root remains positive. We have used the abbreviation

$$\eta_q = \cosh^2\mu_q + \sinh^2\mu_q. \quad (37)$$

It is interesting to compare Eq. (36) with the result arrived at when the coupling between the spin waves $n\mathbf{q}$ with $n \neq 0$ is neglected. The uniform precession is then coupled only to the waves $+\mathbf{q}$ and $-\mathbf{q}$. From Eqs. (11) and (12) with $\langle A^2 \rangle = \tfrac{1}{2}A_q^2$ we get

$$1/T = 2(2\pi/\hbar)(\tfrac{1}{2}\gamma\hbar A_q)^2 \cosh^2\mu_q \, \delta(\hbar\omega_0 - \hbar\omega_q). \quad (38)$$

Comparison of Eqs. (36) and (38) shows that owing to the coupling between the spin waves the δ function has been replaced by a normalized density-of-states function $\rho(\hbar\omega)$,

$$\rho(\hbar\omega) = (2/\pi)[(\gamma\hbar A_q)^2\eta_q^2 - (\hbar\omega - \hbar\omega_q)^2]^{1/2}/ (\gamma\hbar A_q\eta_q)^2. \quad (39)$$

In the derivation, we have considered H and thus, ω_q, to be constant, whereas ω was variable. We may just as well keep the frequency constant and vary the magnetic field H and with it $\omega_q = \omega_q(H)$. Let the field H_q be defined by

$$\omega_q(H_q) = \omega. \quad (40)$$

For small values of $(H - H_q)$ we may expand the equation

$$\omega_q(H) = \omega_q(H_q) + (H - H_q)\left(\frac{\partial\omega_q}{\partial H}\right)_{H=H_q} + \cdots$$

$$\simeq \omega + \gamma(H - H_q)\eta_q$$

to obtain

$$1/\gamma T = 2(\cosh^2\mu_q/\eta_q)[A_q^2 - (H - H_q)^2]^{1/2}, \quad (41)$$

which is the same result as obtained in Sec. V A for the W function. Now $2\{A_q^2 - [H - (\omega/\gamma)]^2\}^{1/2}$ equals the W function as found in the IG model with an anisotropy field of the form (23). Therefore, the density-of-states function ρ, considered as a function of H, equals $1/\eta_q$ times the W function as found in the IG model normalized to 1, and centered on H_q instead of ω/γ. In terms of magnetic field, the spin waves $\mathbf{q}$ and $-\mathbf{q}$ are broadened over the range from $H_q - A_q$ up to $H_q + A_q$. No dipolar narrowing occurs, which must be understood from the fact that the anisotropy field couples the states $n\mathbf{q}$, and for all of these the contribution of the
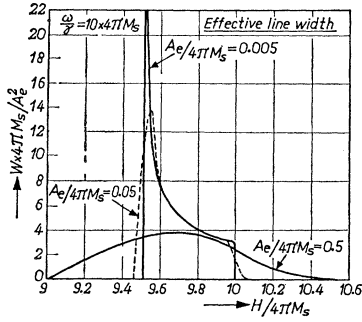
FIG. 12. $W \times 4\pi M_s/A_e^2$ versus $H/4\pi M_s$ for constant frequency $\omega = 10 \times \gamma 4\pi M_s$ and various values of $A_e/4\pi M_s$. With increasing A_e values the influence of the SW manifold disappears and finally the W curve resembles that for one A_q term, as presented in Fig. 11.

dipolar interaction to their energy is the same (the exchange energy is still neglected).

C. Generalization of Simple Model

A nonuniform anisotropy field $A(\mathbf{r})$ broadens the SW frequencies. As found in Secs. V A and V B, the broadening of the relevant spin waves could easily be calculated for the simple model where $A(\mathbf{r}) = A_q \cos\mathbf{q} \cdot \mathbf{r}$. The calculation was easy, because only a set of degenerate spin waves had to be considered. For such degenerate spin waves the broadening is of first order and extends over the full range of field variations $2A_q$.

For the general case, where $A(\mathbf{r}) = \sum_k A_k e^{i\mathbf{k} \cdot \mathbf{r}}$, the spin waves to which the uniform precession is coupled will themselves be coupled to other spin waves, both of the same and of different frequencies. The broadening of the relevant spin waves is then partly of first and partly of higher order, and an exact calculation becomes extremely difficult. We shall restrict ourselves to a generalization of the simple-model result.

For the simple model, the result (38) is modified into (41). We propose to apply a similar modification to the result (11). This can be done straightforwardly by replacing the quantity A_q^2 for the simple model by $2\langle A^2 \rangle \equiv A_e^2$ in the general case. One finds that

$$W = 1/\gamma T = \int_0^{\pi/2} \sin\theta_k \, d\theta_k (\cosh^2\mu_k/\eta_k)$$
$$\times \{A_e^2 - [H - H(\theta_k)]^2\}^{1/2}. \quad (42)$$

The result of this integration is shown in Fig. 12, where $W 4\pi M_s/A_e^2$ has been plotted as a function of $H/4\pi M_s$ for several values of $A_e/4\pi M_s$ at fixed frequency $(\omega/\gamma = 10 \times 4\pi M_s)$. The intrinsic damping of the spin waves has been put equal to zero.

Qualitatively, the W curves change drastically with increasing A_e. For $A_e/4\pi M_s = 0.005$, one recognizes the curves from the first-order theory, given by the dashed lines in Figs. 5–9. W is nonzero only inside the

SW manifold. For $A_e/4\pi M_s = 0.05$, the peak of the curve is reduced and W is seen to decrease gradually to zero outside the limits of the undisturbed SW manifold.

For $A_e = 0.5 \times 4\pi M_s$ no trace is left of the maximum at the lower limit of the SW manifold. A broad maximum is observed, which for large A_e values changes into the half-circle shown in Fig. 11 for the case of one Fourier component. In this limit the exact location of the SW manifold is irrelevant. One finds the results of the IG model for a distribution function corresponding to the sinusoidal variation of $A(\mathbf{r})$. In Sec. V E, a modification will be proposed to introduce some features of the correct distribution function for cubic anisotropy into the W curves for large A values.

The variation of the shape of the W curves in Fig. 12 does not affect the integral of W over the magnetic field, which is still given by Eq. (15).

Consider now the quantitative relation between W and A_e. For small A_e the variation of W with A_e depends on the value of the magnetic field. At the high-field limit of the SW manifold W is given by [cf. (13)]

$$W = \pi\omega A_e^2/4\pi M_s\omega_i. \quad (43)$$

This result is also found in the first-order theory.

At the low-field limit the value of W is finite in contrast to first-order theory. In formula,

$$W = 3.6(A_e^2/4\pi M_s)(4\pi M_s/A_e)^{1/2}. \quad (44)$$

The expression (44) has been written in this particular way for comparison with two formulas given by Schlömann.[5] In order to remove the singularity, he considered the case of finite intrinsic damping, given by a linewidth ΔH_i, and the case where the exchange term cannot be neglected. In the first case, W is given by

$$W = 1.5(H_a^2/4\pi M_s)(4\pi M_s/\Delta H_i)^{1/2}, \quad (45)$$

whereas the presence of the exchange field H_{ex} leads to

$$W = (H_a^2/4\pi M_s)[4\pi M_s/H_{ex}(a^2/r_0^2)]^{1/2}, \quad (46)$$

where a is the lattice constant and r_0 a measure of the grain diameter.[5]

In the result given by Eq. (44), W is no longer proportional to the square, but to the $\frac{3}{2}$ power of the rms anisotropy field.

At the limits of the SW manifold, Fig. 12 shows that, for small values of $A_e/4\pi M_s$, W decreases linearly to zero, as a function of H. The range of field over which this occurs is given by A_e. Indeed, in our model, the dipolar narrowing is effective for the uniform precession, but not for the spin waves, which are broadened over the full range.

Our results can be compared with a recent theory of Schlömann's.[25] Since the results are different in some

[25] E. Schlömann, J. Appl. Phys. **40**, 1199 (1969); Phys. Rev. **182**, 632 (1969).

details, it is worth considering these differences and their origin.

The uniform precession is coupled to spin waves with $k \approx r_0^{-1}$, where r_0 is the average grain size. The question is: By how much are the energies of such spin waves themselves broadened? It is difficult to determine accurately the broadening for $k \approx r_0^{-1}$, but, as Schlömann pointed out, it is easily done for $k \ll r_0^{-1}$, or for $k \gg r_0^{-1}$.

Spin waves with $k \ll r_0^{-1}$ are very similar to the uniform precession and their frequencies will be broadened by the same amount γW. Spin waves with $k \gg r_0^{-1}$ are coupled by $A(\mathbf{r})$ to nearly parallel spin waves, with nearly the same frequencies. The disturbance now produces the full amount of broadening; there is no dipolar narrowing for such spin waves.

Schlömann[25] has used a self-consistent treatment in which the spin waves are assumed to have the same linewidth as the uniform precession; it corresponds to $k \ll r_0^{-1}$. In our treatment the spin waves were assumed to be broadened over the full range of field variations; this corresponds to $k \gg r_0^{-1}$. The relevant spin waves have $k \approx r_0^{-1}$, and their broadening should be somewhere in between that for $k \ll r_0^{-1}$ and that for $k \gg r_0^{-1}$. The two treatments yield the same result inside the SW manifold, but significant differences are found near the limits. In our case (Fig. 12), W decreases to zero over a range of magnetic fields equal to A_e, whereas in Schlömann's treatment, this field range is of the order of the value of W inside the manifold.

Another difference is found in the maximum value of W. Schlömann's result is proportional to $H_a^{4/3}$, whereas (44) gives a factor $H_a^{3/2}$.

One may expect the correct results to lie somewhere in between these limits.

D. Comparison with Experiment

In order to compare the theoretical results with the data in Figs. 5–9 two parameters have to be chosen—the intrinsic damping and the value of A_e. As before, the magnitude of the intrinsic damping will be derived from the high-field W value. This intrinsic damping has been incorporated into the equations of motion.

The A_e values that have been used in calculating the drawn lines in Figs. 5–9 are given in Table I in the column labeled A_e(expt).

These A_e values should be compared with the values derived from the relation $A_e^2 = 2\langle A^2 \rangle$, where $\langle A^2 \rangle$ can be expressed in terms of first-[5] and second-order anisotropy constants K_1 and K_2. These quantities are known from static measurements on single crystals.[12,13] Their values for $Ni_{1-x}Co_xFe_2O_4$ are $K_1 = (-7 + 260x) \times 10^4$ erg/cm^3 and $K_2 = -400x \times 10^4$ erg/cm^3. For x larger than 0.01, $|K_2|$ is bigger than $|K_1|$.

The anisotropy field can be expressed in K_1, K_2, and the direction cosines of the magnetization $(\alpha_1, \alpha_2, \alpha_3)$ with respect to the cube edges [100], [010], and [001]. One finds that

$$A(\alpha_1, \alpha_2, \alpha_3) = [2K_1 + (K_2 - 10K_1)$$
$$\times \sum_{i > j} \alpha_i^2 \alpha_j^2 - 21K_2 \alpha_1^2 \alpha_2^2 \alpha_3^2]/M_s. \quad (47)$$

The average value of A^2 is then found to be

$$\langle A^2 \rangle = (16/21)[K_1^2 + (2/11)K_1K_2$$
$$+ (5/143)K_2^2]/M_s^2. \quad (48)$$

Using $A_e^2 = 2\langle A^2 \rangle$, (48), and the single-crystal data on K_1 and K_2, one finds the A_e(theor) values given in Table I. A reasonable agreement is found with A_e(expt).

For $x = 0.027$, one may note that $K_1 = 0$ and therefore, that the drawn curve shown in Fig. 8 is determined by the K_2 value and the intrinsic damping.

The experimental data shown in Figs. 6–9 are in good agreement with the modified theory. In particular, the heights of the peaks in the W and S curves show a good fit. The gradual decrease of W outside the limits of the SW manifold is also well described.

Agreement between theory and experiment for $x = 0$ (Fig. 5) is rather bad, whereas for $x = 0.05$, with a 12% smaller A_e value, the agreement is much better. We do not believe that the discrepancy for $x = 0$ can be ascribed to porosity ($p = 0.36 \times 10^{-2}$) or to chemical inhomogeneity, since spray drying gives very homogeneous materials. Moreover, the results were exactly the same for a second nickel ferrite. Another argument is that $\int W \, dH$ [cf. the relation (15)] has the correct value. Since these experiments were performed, similar curves have been observed in Mg ferrite[26] and in YCaV garnet,[11] with comparable $A_e/4\pi M_s$ values. At the present time the theory has not been extended far enough to account accurately for the S and W curves of Fig. 5.

In the theories discussed so far, the sign of K_1 was unimportant, since only quadratic relations in A_e were used. The experimental data, however, give some indication that the sign of K_1 might be of some importance. In Fig. 9, one notes that in the first case, where $K_1 > 0$, the experimental data are found to be shifted slightly to lower-field values in comparison to the theoretical curve. In Fig. 5, where $K_1 < 0$, the maximum in the W curve is shifted to higher-field values. In Sec. V E, special attention will be paid to the cubic aspects of the variations in anisotropy field.

Having considered so far the details of the effective linewidth W and the line shift S, we now turn to the normal linewidth ΔH (Fig. 4). ΔH is related by (18) of Sec. II to W_{res}, the W value at the field for resonance at 9005 MHz, and to ΔS, the difference in S values found at the magnetic fields where χ'' is half its maxi-

[26] Q. H. F. Vrehen, H. G. Beljers, and J. G. M. de Lau IEEE Trans. Mag. **5**, 617 (1969).
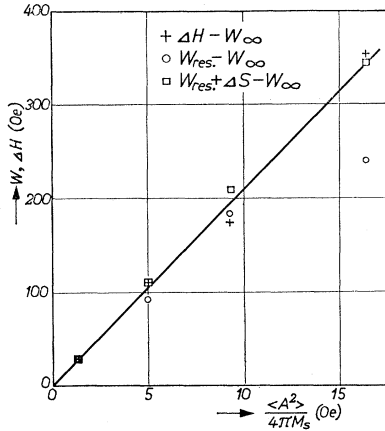
FIG. 13. $\Delta H - W_\infty$ (crosses), $W(H_{res}) - W_\infty$ (open circles) and $W(H_{res}) - W_\infty + \Delta S$ (squares) as a function of $\langle A^2\rangle/4\pi M_s$.

mum value. In order to compare ΔH and W_{res} with anisotropy broadening theory, a correction for the intrinsic damping has been applied to both quantities by subtracting W_∞, the W value at 6 kOe. Figure 13 shows a plot of $\Delta H - W_\infty$, $W_{res} - W_\infty$, and $W_{res} + \Delta S - W_\infty$ against $\langle A^2\rangle/4\pi M_s$ as determined from (18) and the K_1 and K_2 values given above.

For small A values the ΔS correction is not important and good agreement is found between ΔH and W_{res}. For the highest A value (NiFe$_2$O$_4$) the ΔS correction of about 100 Oe is necessary.

In Fig. 13, the slope of the straight line is 20, which should be compared to a value of 33 in Schlömann's theory.[5] Since the SW broadening reduces the peak of the W curve, this reduction of the linewidth for resonance on a sphere is not surprising.

E. Large Cubic Anisotropy

In this part, the case of relatively large cubic anisotropy fields, $H_a \gtrsim 4\pi M_s$, will be considered. In Secs. V A–V D the anisotropy field entered into the final expressions only through the quantity $\langle A^2(\mathbf{r})\rangle$. In the following, the detailed distribution function of the anisotropy fields for cubic anisotropy will be needed.

The effects of the anisotropy will again be described by an additional field $A(\mathbf{r})$ parallel to H. For cubic anisotropy this is valid if $\omega \gg \gamma H_a$. Exchange interactions will be neglected as before.

First consider the case where $H_a \gg 4\pi M_s$ so that the dipolar interactions are unimportant. The effective linewidth and line shift may then be calculated in the IG model. From the anisotropy field distribution given by Schlömann,[3] the real and imaginary parts of χ_+ may be calculated with Eqs. (2)–(4). The distribution depends on the ratio $\gamma H_a/\omega$, and the calculation was made for $\gamma H_a/\omega = 0.18$, the value appropriate for NiFe$_2$O$_4$ at 9000 MHz. The result is shown in Fig. 14, where χ_+' and χ_+'' have been plotted as a function of

$(H - \omega/\gamma)/(2K_1/M_s)$. The singularity in χ_+'' is due to grains for which $H \| [110]$. At the field limits $H = (\omega/\gamma) - \frac{2}{3}H_a$ and $H = (\omega/\gamma) + H_a$, the susceptibility χ_+'' arises from grains for which $H \| [111]$ and $H \| [100]$, respectively. The picture has been drawn for $K_1 < 0$. For positive anisotropy the abscissa changes sign, thereby changing the center of gravity from -0.04 to $+0.04$.

The effective linewidth W_{IG} and line shift S_{IG} can now be calculated formally from Eqs. (16) and (17). The result in Fig. 15 shows that the singularity in χ_+'' has led to a zero in W_{IG} and to a discontinuity in S_{IG}. Curves similar to those for W_{IG} and S_{IG} must be expected for W and S for $H_a \gg 4\pi M_s$.

The integral of W_{IG} over the frequency can be shown[27] to be proportional to the second moment of the absorption $\chi''(\omega)$, just as in the SW model, Thus,

$$\int_{-\infty}^{+\infty} W_{IG}\, d\omega = \frac{2}{M_s}\int_{-\infty}^{+\infty} \chi''(\omega)(\omega - \bar\omega)^2\, d\omega = 2\pi\gamma\langle A^2\rangle. \tag{49}$$

The second equality follows from Eqs. (3) and (4).

For the case $H_a \simeq 4\pi M_s$, it is very difficult to make a detailed calculation of W and S. On the basis of the insight gained in the Secs. V A–V C, we now put forward some qualitative arguments leading to expressions from which W and S may be calculated with fair success in this intermediate range. We note that we have already assumed $\omega \gg \gamma H_a$. Since, furthermore, $H_a \simeq 4\pi M_s$, we have $\omega \gg \gamma 4\pi M$ so that in Eqs. (37)–(41) we may put $\cosh\mu_q = \eta_q = 1$.

In Secs. V A and V B, we found that for a simple sinusoidal variation of $A(\mathbf{r})$, the interaction between spin waves could be taken into account by replacing the δ function for the SW frequency by an appropriate density-of-states function. This density-of-states function was just equal to the normalized W function as calculated for that particular anisotropy field distribution in the IG model.
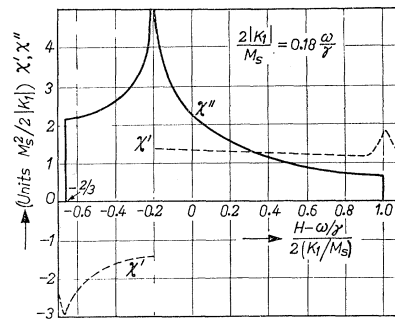

FIG. 14. χ_+' and χ_+'', as a function of $H - \omega/\gamma$, calculated for the IG model and for first-order anisotropy. $H_a \equiv 2|K_1|/M_s$ has been taken equal to 0.18 ω/γ.

[27] The proof can be given by function-theoretical methods [J. A. Geurst (private communication)].

The appearance of this feature of the IG model was understood from the fact that the interacting spin waves were all degenerate in the absence of $A(\mathbf{r})$. A similar density-of-states function was then used (Sec. V C) for the case of many Fourier components present in $A(\mathbf{r})$. It was also indicated that in the latter case the width of the density-of-states function was probably somewhat overestimated because some dipolar narrowing should occur. This narrowing should become less important when H_a increases with respect to $4\pi M_s$. Thus, for $H_a \geqslant 4\pi M_s$, we expect to find good results simply by replacing the δ function at the SW frequency by a normalized W function calculated on the basis of the IG model.

Instead of using the density of (39) which is valid for a cosine variation of $A(\mathbf{r})$, we must use the normalized W_{IG} function for cubic anisotropy, which has been given above in Fig. 15. Thus, we use the function $w(\omega - \gamma H)$ defined by

$$w(\omega - \gamma H) \equiv W_{IG}(\omega - \gamma H) \Big/ \int W_{IG}(\omega - \gamma H) d\omega$$

$$= W_{IG}(\omega - \gamma H)/2\pi\gamma\langle A^2 \rangle, \quad (50)$$

where Eq. (49) has been used. Replacing the δ function in Eq. (11) by $w(\omega - \omega(\theta))$ one obtains

$$W = \frac{1}{\gamma T} = 2\pi\gamma\langle A^2 \rangle \int_0^{\pi/2} w(\omega - \omega(\theta)) \sin\theta \, d\theta, \quad (51)$$

where $\cosh\mu(\theta) = 1$ has been substituted in Eq. (12). Similarly,

$$S = -\langle A(\mathbf{r}) \rangle - \gamma\langle A^2 \rangle \int_{-\infty}^{+\infty} d\omega' \int_0^{\pi/2} \frac{w(\omega' - \omega(\theta))}{\omega - \omega'}$$

$$\times \sin\theta d\theta. \quad (52)$$

The expressions (51) and (52) are correct for both limits $H_a \gg 4\pi M_s$ and $H_a \ll 4\pi M_s$, provided $\omega \gg \omega_m$. For
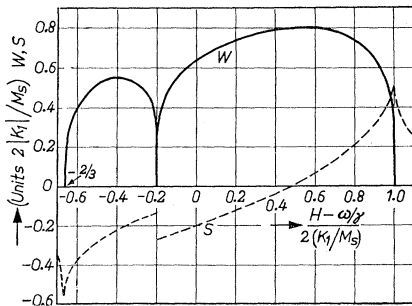
FIG. 15. W and S as a function of $H - \omega/\gamma$, as calculated from the susceptibility shown in Fig. 14.
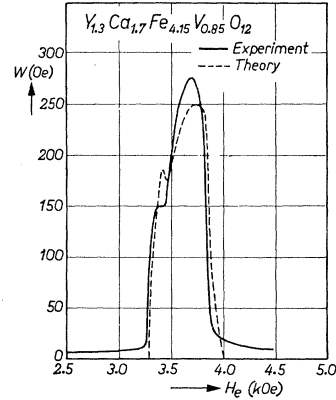
FIG. 16. W versus H_e for $Y_{1.3}Ca_{1.7}Fe_{4.15}V_{0.85}O_{12}$, for which $4\pi M_s = 265$ G and $H_a = 350$ Oe. Experimental results of Patton's (Ref. 11) are compared with theory [Eq. (51)].

$H_a \gg 4\pi M_s$ this can readily be seen from Eq. (50) by using $\omega(\theta) = \gamma H$, since dipolar effects are now neglected. For $H_a \ll 4\pi M_s$, the density $w(\omega - \omega(\theta))$ becomes very narrow and approaches the δ function in (11) [$\cosh\mu(\theta) = 1$ in our present approximation].

Since the expressions (51) and (52) are valid for $H_a \ll 4\pi M_s$ and for $H_a \gg 4\pi M_s$, one might hope that they are also of use in the intermediate range. It turns out that for $NiFe_2O_4$, where $H_a/4\pi M_s = 0.16$, Eq. (51) does not describe the experiments any better than Eq. (42). The discrepancy between theory and experiment for this ferrite is, therefore, not removed by the considerations presented in this section. Much better agreement is found for a material where $H_a \geqslant 4\pi M_s$, namely, for $Y_{1.3}Ca_{1.7}Fe_{4.15}V_{0.85}O_{12}$. The effective linewidth of this ferrimagnet, which has the garnet structure, and for which $H_a = 350$ Oe and $4\pi M_s = 265$ G, was recently measured by Patton. With his kind permission his data are reproduced in Fig. 16, together with a theoretical curve calculated with Eq. (51). Satisfactory agreement exists.

It may be concluded that the extension of the theory proposed in this section works satisfactorily for $H_a \gtrsim 4\pi M_s$, and it is precisely for this range that the theory was made. The modification of the theory does not improve the agreement between theory and experiment for $H_a/4\pi M_s \simeq 0.15$.

VI. CONCLUSION

Our results can be summarized as follows: (1) The use of the quantities W and S allows a detailed comparison of experiment and theory, both with the SW model and the IG model. The usual linewidth ΔH depends both on W and S (Sec. IV). (2) Experimental data on dense NiCo ferrites have shown that, outside the limits of the SW manifold, defined by (10), W is independent of magnetic field, but a monotonically increasing function of Co content (Fig. 10). The relaxa-

tion due to Co^{2+} ions can therefore not be described by a two-magnon process. (3) Experimental results on W and S well inside the limits of the SW manifold show quantitative agreement with Schlömann's theory[5] as long as $H_a/4\pi M_s \lesssim 0.1$ (Figs. 5–8). For Ni ferrite this quantity equals 0.16 and no agreement is found (Fig. 5). (4) The singularities and discontinuities in W and S, as predicted by Schlömann's theory at the limits of the manifold, were not observed experimentally. This led to a consideration in Sec. V of the SW modes in a non-uniform internal field. For a sinusoidal variation of $A(r)$, the result is that the density of states of a spin wave is broadened over the full variation of the internal field [as in (39)]. The result has been generalized to the case where $A(r)$ contains many Fourier components by assuming that the spin waves are broadened over a field range $2\langle A^2(r)\rangle^{1/2}$. Good agreement with the experimental data was obtained, except for nickel ferrite. (5) An attempt was made to consider the case of large anisotropy, where the cubic features of the IG model were incorporated in the density-of-states function (Fig. 15). The result agreed well with Patton's[11] data (Fig. 16), but again did not with those of Fig. 5 for nickel ferrite. In conclusion, Eq. (42) described the experiments well for $(H_a/4\pi M_s) \lesssim 0.1$, and Eq. (51) does so for $(H_a/4\pi M_s) \gtrsim 1$. For Ni ferrite and Mg ferrite, which have $(H_a/4\pi M_s) \approx 0.15$–$0.2$, neither (42) nor (51) leads to quantitative agreement with experiment. The reason is unknown.

ACKNOWLEDGMENTS

APPENDIX

In this Appendix, we present the calculation of the susceptibility $\chi_+ \equiv \langle m_+(r)\rangle / h_+^{(e)}$, of a system described by (24), where the demagnetizing field is given by (27).

In terms of the circularly polarized components $m_\pm(r)$ and $h_\pm(r)$, defined as $m_\pm = m_x \pm im_y$ and $h_\pm = h_x \pm ih_y$, Eq. (24) becomes

$$\pm(\omega/\gamma)m_\pm(r) = [H + A_q \cos(q\cdot r) + i\lambda]m_\pm(r) - M_s[h_\pm^{(e)} + h_\pm^{(d)}(r)], \quad (A1)$$

where $\lambda = \omega\alpha/\gamma$. In terms of the Fourier components of $m(r)$ and $h(r)$, Eq. (A1) reads

$$[H \pm \omega/\gamma + i\lambda]\mathfrak{m}_\pm(k) + \tfrac{1}{2}A_q[\mathfrak{m}_\pm(k+q) + \mathfrak{m}_\pm(k-q)] = M_s[h_\pm^{(e)}\delta_{k,0} + h_\pm^{(d)}(k)], \quad (A2)$$

where

$$h_\pm^{(d)}(k) = -4\pi N\mathfrak{m}_\pm(0)\delta_{k,0} - 4\pi k_\pm[\mathfrak{m}(k)\cdot k]/|k|^2. \quad (A3)$$

From (A2) and (A3) the component $\mathfrak{m}(k)$ is seen to be coupled to the components $\mathfrak{m}(k+nq)$, where n is any integer. The equations for $\mathfrak{m}(k+nq)$, with a fixed $k \neq nq$ and all values of n, are homogeneous. For a finite value of λ, therefore, $\mathfrak{m}(k) = 0$ for these k values. The general solution $\mathfrak{m}(r)$ may thus be written

$$m(r) = \sum_{n=-\infty}^{+\infty} \mathfrak{m}(n)e^{inq\cdot r} \equiv m(q\cdot r). \quad (A4)$$

The demagnetizing field (27) can now be written as

$$h^{(d)} = -4\pi \sin^2\theta_q e_1 \sum_{n\neq 0} [m(n)\cdot e_1]e^{inq\cdot r} - 4\pi Nm(0)$$

$$= -4\pi \sin^2\theta_q e_1\{[m(q\cdot r) - \mathfrak{m}(0)]\cdot e_1\} - 4\pi Nm(0), \quad (A5)$$

where e_1 is a unit vector along the projection of q on the xy plane. Choosing a new x axis along e_1 we can write for the circularly polarized components

$$h_\pm^{(d)} = -2\pi \sin^2\theta_q[m_\pm(q\cdot r) + m_\mp(q\cdot r) - \mathfrak{m}_\pm(0) - \mathfrak{m}_\mp(0)] - 4\pi N\mathfrak{m}_\pm(0).$$

After substituting into (A1), one finds that

$$[H + A_q \cos(q\cdot r) + i\lambda \mp \omega/\gamma]m_\pm(q\cdot r)$$
$$= M_s\{h_\pm^{(e)} - 4\pi N\mathfrak{m}_\pm(0) - 2\pi \sin^2\theta_q$$
$$\times [m_\pm(q\cdot r) + m_\mp(q\cdot r) - \mathfrak{m}_\pm(0) - \mathfrak{m}_\mp(0)]\}.$$

After rearranging terms, this becomes

$$[H + A_q \cos(q\cdot r) + i\lambda \mp \omega/\gamma + 2\pi M_s \sin^2\theta_q]m_\pm(q\cdot r)$$
$$+ 2\pi M_s \sin^2\theta_q m_\mp(q\cdot r) = M_s\{h_\pm^{(e)} - 4\pi N\mathfrak{m}_\pm(0)$$
$$+ 2\pi \sin^2\theta_q[\mathfrak{m}_\pm(0) + \mathfrak{m}_\mp(0)]\} \equiv M_s K_\pm. \quad (A6)$$

Since the right-hand side of (A6) is independent of r, two components $K_\pm$ of a vector K have been introduced. Solving for $m_\pm(r)$, one finds an expression of the following form:

$$m(r) = \chi(r)\cdot K. \quad (A7)$$

It is not difficult to see that $\chi(r)$ has a component with a sharp peak at those values of r for which the angular frequency ω and the total field

$$H(q\cdot r) \equiv H + A_q \cos(q\cdot r)$$

satisfy

$$\omega = \gamma\{H(q\cdot r)[H(q\cdot r) + 4\pi M_s \sin^2\theta_q]\}^{1/2}.$$

A similar result is found in the IG model, provided $M_s \sin^2\theta_q$ is put equal to zero.

The uniform precession can be obtained from (A7) by taking the integral over r. After some elementary

algebra, one finds that this involves integrals of the following type:

$$I(c_{\pm}) = \int_0^{2\pi} dx [c_{\pm} + i\lambda\gamma + \gamma A_q \cos x]^{-1},$$

where

$$c_{\pm} = \gamma H_0 + B \pm (\omega^2 + B^2)^{1/2}$$

and

$$B = 2\pi\gamma M_s \sin^2\theta_q.$$

For $|c| > A_q$ one has

$$2\pi/I(c) = \mathrm{sgn}(c)(c^2 - \gamma^2 A_q^2)^{1/2} + i\gamma\lambda c/(c^2 - \gamma^2 A_q^2)^{1/2}, \quad \text{(A8)}$$

for $|c| < A_q$, one has

$$2\pi/I(c) = i(\gamma^2 A_q^2 - c^2)^{1/2} + \gamma\lambda c/(\gamma^2 A_q^2 - c^2)^{1/2}. \quad \text{(A9)}$$

Using (A8) and (A9) and eliminating K_+ and K_- by (A6), one derives expressions for the uniform precession $\mathfrak{m}_{\pm}(0)$, the susceptibility $\chi_{\pm}$ and the quantities S and W. Neglecting the nonresonant contribution from $I(c_+)$, one recognizes the semicircular shape of the $W(H)$ curve in Fig. 11 in the imaginary part of (A9). For vanishing λ, the only contribution to W comes from the field range $H = H_q \pm A_q$, where $H_q = (\omega^2 + B^2)^{1/2} - B$.

For the integration described in Sec. V C the quantities S and W for finite λ were integrated numerically in order to derive the drawn lines in Figs. 5–9.